Designing Short Term Wave Traces to Assess Wave Power Devices

Designing Short Term Wave Traces to Assess Wave Power Devices

Pál Schmitt[1], *Lucas Danisch*[2], *Paul Lamont-Kane*[1], *Björn Elsäßer*[1]

[1]Queen's University Belfast
Portaferry
Northern Ireland

[2]TU Hamburg-Harburg
Hamburg
Germany

ABSTRACT

In recent years modern numerical methods have been employed in the design of Wave Energy Converters (WECs), however the high computational costs associated with their use makes it prohibitive to undertake simulations involving statistically relevant numbers of wave cycles. Experimental tests in wave tanks could also be performed more efficiently and economically if short time traces, consisting of only a few wave cycles, could be used to evaluate the hydrodynamic characteristics of a particular device or design modification. Ideally, accurate estimations of device performance could be made utilizing results obtained from investigations with a relatively small number of wave cycles. However the difficulty here is that many WECs, such as the Oscillating Wave Surge Converter (OWSC), exhibit significant non-linearity in their response. Thus it is challenging to make accurate predictions of annual energy yield for a given spectral sea state using short duration realisations of that sea. This is because the non-linear device response to particular phase couplings of sinusoidal components within those time traces might influence the estimate of mean power capture obtained. As a result it is generally accepted that the most appropriate estimate of mean power capture for a sea state be obtained over many hundreds (or thousands) of wave cycles. This ensures that the potential influence of phase locking is negligible in comparison to the predictions made. In this paper, potential methods of providing reasonable estimates of relative variations in device performance using short duration sea states are introduced. The aim of the work is to establish the shortness of sea state required to provide statistically significant estimations of the mean power capture of a particular type of Wave Energy Converter. The results show that carefully selected wave traces can be used to reliably assess variations in power output due to changes in the hydrodynamic design or wave climate.

KEY WORDS: Sea State; Wave trace; Experimental tank testing; wave parameters; non-linear effects; statistics.

INTRODUCTION

The methods used in this work are exampled for the case of a large, surface-piercing Oscillating Wave Surge Converter (OWSC). However, they should be equally applicable for the investigation of other structures deployed in the marine environment. The specific OWSC being considered is a simplified version of the Oyster, a device developed by Aquamarine Power Ltd. following its conception at Queen's University Belfast. The device is designed to be deployed in the near shore region in water depths of around 12-15meter and utilizes the amplified surge motion of water surface waves in this region to pitch back and forward about a hinge mounted on the seabed. The Oyster 800 prototype used 2 double acting hydraulic cylinders to pump high pressure fresh water to an onshore power plant, in turn generating electricity through the use of a conventional Pelton wheel turbine. The basic concept is shown in figure 1.

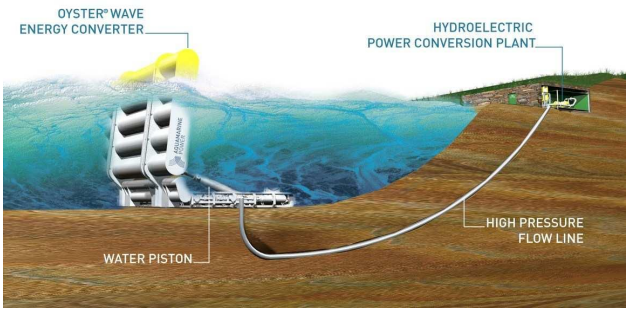

Fig. 1 Conceptual sketch of Oyster 1 (Aquamarine Power Ltd, 2015)

One of the most common methods used in the development of WECs is physical experimentation undertaken in a wave tank which can be both time consuming and expensive. For example, one major improvement on the design of Oyster 1 was the inclusion of end effectors on the Oyster 800.These increase the thickness of the edges of the flap and reduce energy loss due to viscous effects (Figure 2), which has previously been shown to increase power capture (Cameron et al., 2010).
Conducting a study to optimize the contour of these end-effectors requires multiple shapes to be designed, manufactured and tested, all of

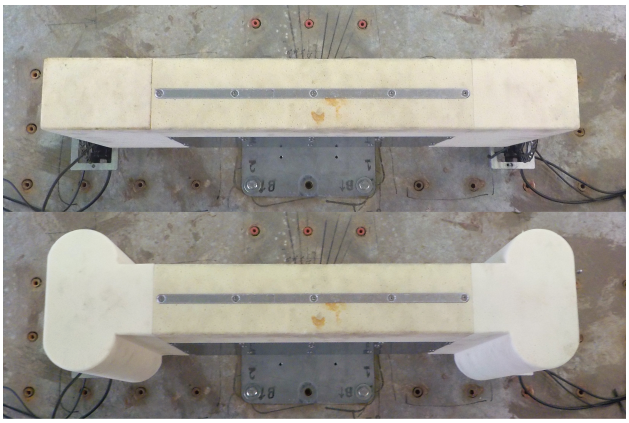

Fig. 2 40^{th} scale model of common box shaped flap (top) and with end-effectors (bottom)

which utilizes human and monetary resources. An advanced computational fluid dynamics (CFD) tool could analyse multiple designs and provide information about which parameter changes are favourable. Simulations eliminate the material costs and would not need any further attention until the simulation has finished. The utilization of CFD has become general practice in many areas of marine engineering. Correctly used, CFD tools achieve results with accuracy close to that of physical testing (Schmitt and Elsaesser, 2015). However, in an industrial setting, and in contrast to experimental testing, CFD tools are still not capable of obtaining results for long duration wave traces at a comparable cost (Schmitt et al., 2012).

A 40^{th} scale model of Oyster moving in a monochromatic sea for 12 to 20s for instance, require approximately 24h of simulation time on a high performance cluster comprising 1.2 to 1.8 million cells running parallel on 32 cores (Asmuth, 2014). Nonetheless this relatively long simulation time is acceptable considering how much time passes from sending blueprints to a workshop to receiving the built model and finally carrying out the experiments. However, to receive valid and statistically significant data, calibrated seas often have run times longer than 256s. It is evident that simulations of that length would be unfeasible in CFD in an industrial context.

In this work different metrics of a surface elevation of a sea state were compared in order to identify a short excerpt within a full sea state that yields the same power output characteristics. Therefore a method was developed to generate sea states numerically from ocean-wave spectra. Subsequently a study was conducted on how specific metrics like significant wave height and mean period of a sea state converge with increasing length of the individual sea state. The analysis was then applied to data obtained from experimental wave tank tests for two different flap shapes and sea states. Particular emphasis was placed on the maximum power output deduced from power curves for different damping coefficients. Results now allow to run CFD simulations for a limited number of waves providing an outcome within a defined level of accuracy.

MATHEMATICAL DESCRIPTION OF A SEA STATE

Sea waves form a unique surface elevation η which can, according to linear theory, be described by a superposition of an infinite number of sinusoidal waves.

Mathematically the surface elevation η of the ocean can therefore be defined as the sum of an infinite amount of sinusoids

$$\eta = \sum_{n=1}^{k} A_n \sin\left(-2\pi f_n t + \varphi_n\right) \tag{1}$$

with individual amplitudes A_n, frequencies f_n and random phase shifts φ_n. The time vector is given by t. The spectral density S_n for each amplitude component A_n derives from the following equation:

$$S_n = \frac{A_n^2}{2df} \tag{2}$$

Several metrics are available by analysing a given time trace of a surface elevation. Metrics of this kind will be referred to as analytical or statistical metrics.

- The wave height of a sine curve is the double of the respective amplitude. Wave height H in an irregular time trace is the elevation difference between the trough and the crest whilst crossing zero once, going from positive to negative values (zero up-crossing). The arithmetic mean of all wave heights in a time span will be referred to as $\bar{H}$.
- A metric often used to describe a sea condition is the average wave height of the largest third of all waves $H_{1/3}$ also referred to as significant wave height.
- Mean wave period T_{zm} is defined as the arithmetic mean of the time intervals between zero up-crossing incidents in the surface elevation.

Applying a Fourier Analysis to a given time trace of a surface elevation yields a spectral representation of the sea state. Generally it is displayed as spectral density $S(f)$ over frequency f. Metrics derived from a spectrum will be referred to as spectral metrics. Particularly useful is the spectral moment of the density function. m_i describes the i^{th} moment of the frequency spectrum and is defined as:

$$m_i = \int_0^\infty f^i S(f) df \tag{3}$$

Assuming that the spectrum is narrow-banded the significant wave height can be derived from the spectral moment:

$$H_{m0} = 4\sqrt{m_0} \tag{4}$$

The factor four in front of the square root in equation 4 is only valid for narrow-banded frequency spectra. This relationship yields to overestimations of approximately 1.5-8 percent for more broad banded frequency spectra (Ochi, 1998).

The mean period is calculated by the division of the 0^{th} moment and the 1^{rst} moment as shown in following equation:

$$T_{01} = \frac{m_0}{m_1} \tag{5}$$

Several formulations have been proposed to describe frequency spectra established through analysis from accumulated field data. However spectral characteristics vary depending on the geographical location where the data was recorded. A modification of the *JONSWAP* spectrum which is based on the results of the Joint North Sea Wave Observation Project (Hasselmann et al. (1973) as presented in Goda (2010)) is given here:

$$S(f) = \beta_J H_{m0}^2 T_p^{-4} f^{-5} \exp\left[-\frac{5}{4}\left(T_p f\right)^{-4}\right] \gamma^{\exp\left[\frac{-\left(T_p f-1\right)^2}{2\sigma^2}\right]} \tag{6}$$

with

$$\beta_J = \frac{0.0624}{0.230 + 0.0336\gamma - 0.185\left(1.9+\gamma\right)^{-1}}\left[1.094 - 0.01915 \cdot ln\gamma\right] \tag{7}$$

$$T_p \backsimeq \frac{T_{01}}{1 - 0.532\,(\gamma + 2.5) - 0.569} \tag{8}$$

$$\sigma = \begin{cases} 0.07 : f \leq f_p, \\ 0.09 : f \geq f_p, \end{cases} \tag{9}$$

β is shown here as used in the procedure for wave tank calibration. It is a relationship between fetch length, mean wind speed and gravity. The peak wave period T_p is estimated from T_{01} by equation 8.

GENERATION AND ANALYSIS OF A SEA STATE

The clock rate $CR = 32Hz$ of the wave-maker determines the rate of data output and data sampling in processes like wave generation and device triggering. To operate the tank a run number rn has to be chosen. The run number defines the time interval T_r after which the generated surface elevation repeats.

$$T_r = \frac{2^{rn}}{CR} \tag{10}$$

The time vector t with a sampling rate of dt and a length of T_r was defined to have the same amount of data points $\kappa = 1.3 \cdot 10^5$ for each run number.

$$dt = \frac{T_r}{\kappa} \tag{11}$$

Only frequency components f_n with df as an even-denominator can be implemented in a generated wave trace.

$$f = n \cdot df, n \in \mathbb{N} \tag{12}$$

The inverse of the repeat time gives the frequency interval df between components in the chosen frequency range that may be generated by the wave paddles (Edinburgh Design Ltd., 2014).

$$df = \begin{cases} \frac{1}{T_r}, \\ f_{n+1} - f_n, \end{cases} \tag{13}$$

The frequency range $f_{min} \leqslant f_n \leqslant f_{max}$ is restricted by the memory of the wavemaker and was chosen according to the following conditions:

$$0.002 \geq \int_{0Hz}^{f_{min}} S(f)df \tag{14}$$

$$0.005 \geq \int_{f_{max}}^{8Hz} S(f)df \tag{15}$$

Considering that spectral density is proportional to the energy contained in the respective frequency component an energy loss of 0.7% is accepted by using this method. Due to the large tail of components with higher frequencies, but low spectral density a greater part is cut off on the right side of the integral to achieve an adequate amount of spectral components.
The final spectrum is then computed by inserting the received frequency range f_n into *JONSWAP* equation 6. From the new spectrum the amplitude components are extracted by rearranging equation 2:

$$A_n = \sqrt{2dfS_n} \tag{16}$$

A random initial phase φ_n for each frequency component must be chosen. The hereby defined parameters are then used in equation 1. The result is a unique surface elevation time trace.
The sea states displayed in table 1 are going to be used for this investigation. They were chosen from 47 sea states used by Aquamarine Power Ltd. to describe the wave climate at their EMEC test site.

Table 1 Calibrated sea states. Values are given in full scale.

	Sea04	**Sea10**	**Sea19**
H_{m0} [m]	1.75	1.75	1.75
T_{01} [s]	5.5	7.5	9.5

CONVERGENCE STUDY OF SEA STATE PARAMETERS

Since the phase shift φ of spectral components is applied randomly the statistical properties of numerically generated sea states vary. Therefore a convergence study was conducted for the values of $\bar{H}$, $H_{1/3}$ and T_{zm} for differing initial phase angles. A number of one hundred sea states for nine different lengths, all defined by one *JONSWAP* spectrum computed by the users input of H_{m0} and T_{01} were analysed to see how the standard deviation of the time domain variables develops when the duration of the sea state increases. Power output, the property of interest in this investigation, is expected to be related to those values, but it should be noted that the exact nature of the depence is unknown.
The results for Sea10 are shown in figure 3 and 4. The graphs x-axis show the lengths of the sea states going from 8s to 2048s, doubling in each step. The left y-axis labels the magnitude of the mean values of the corresponding seas shown as circles and connected by a solid line. The standard deviations for each sea state are shown as error bars. The dash-dotted line shows the normalized standard deviation σ to the respective mean value, which converges towards zero with increasing sea length. The dashed lines represent the input values of H_{m0} and T_{01}. Note that the values of $H_{1/3}$ and T_{zm} are considerably lower. This is due to the usage of a spectrum that is not narrow banded (Ochi, 1998). The accuracy of these relations is not part of this investigation.
The graphs help to understand how accurately the input values are matched for a given length of a sea state. They also give an idea of the possible variance of the results of a single test run with the respective duration. The time domain values of short duration sea states with lengths of less than 32s have normalized standard deviations of more than 5%. While sea states of more than 128s already show standard deviations of less than 2,5%. The values of the standard deviations of sea states longer than 2048s are less than 1%.

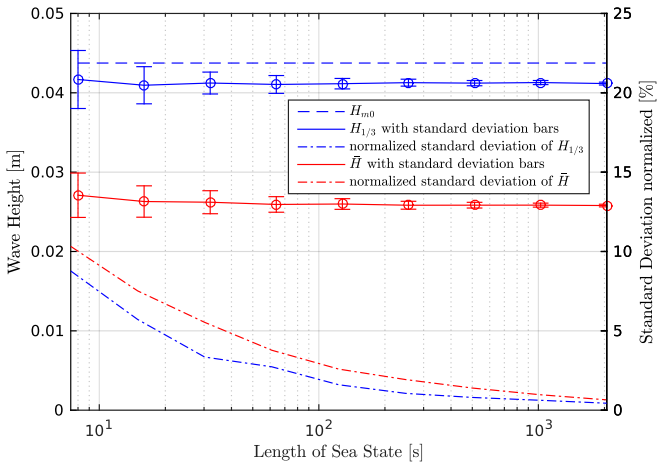

Fig. 3 Showing convergence of $H_{1/3}$ and $\bar{H}$ in generated sea states with length of respective seas

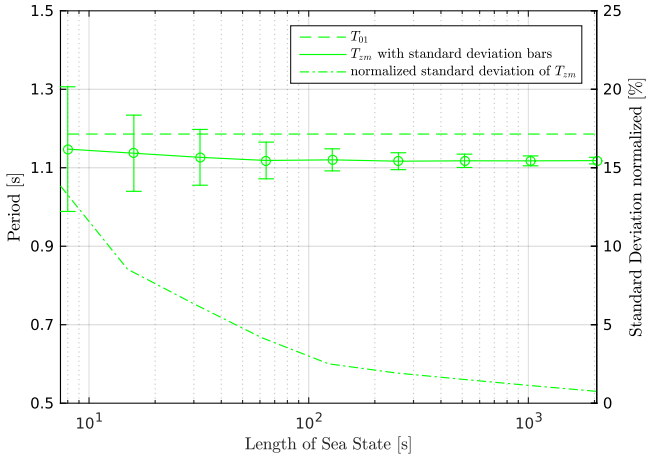

Fig. 4 Showing convergence of T_z in generated sea states with length of corresponding seas

ADVANCED METRICS

Many metrics can be derived from the spectral variance of a given sea state or surface elevation. Especially incident wave power is of interest. However, a Fourier analysis of a short duration elevation trace often contains discrete peaks and is of limited use to derive spectral metrics. Hence time domain metrics were used exclusively in this work. The investigation was performed by comparing metrics of a short length or so called window of surface elevation to the same metric of the entire sea state. The effect of these short wave traces on a WEC was then assessed by comparing average power production during these short time traces to the full scale data.

The following section describes metrics developed in addition to the well known parameters discussed above to analyse the data gained from the experiments. All post processing was performed in MATLAB/octave.

Metric Comparison Method

In wave energy research significant wave height $H_{1/3}$ is often used for calculations. However, this metric describes the mean wave height of only the largest one third of waves. Two thirds of significant data are thus not properly taken into account. One can easily think of examples of wave traces with the same significant wave height but very different overall mean wave heights $\bar{H}$. Mean wave period T_{zm} influences power output as well. Therefore all three were included in a newly developed metric.

This method receives the values of the time domain variables for each window and compares them to the full sea state's values. The significant wave height of the current window $H_{1/3}(w)$ is subtracted from the significant wave height of the whole sea state $H_{1/3,sea}$ and likewise for the other two variables. The absolute of the difference is then divided by the desired value of the whole sea state to receive a proportion of the window's discrepancy. This normalization makes the single discrepancies comparable. They are summed up equally and form the discrepancy metric Δ_m.

$$\Delta_m(w) = \frac{|H_{1/3,sea} - H_{1/3}(w)|}{H_{1/3,sea}} + \frac{|\bar{H}_{sea} - \bar{H}(w)|}{\bar{H}_{sea}} + \frac{|T_{zm,sea} - T_{zm}(w)|}{T_{zm,sea}} \quad (17)$$

However, two of the three summands are values of wave height and only one is a value of wave period. Therefore a change of wave height will influence Δ_m more strongly. A simple weighted average would solve the raised issue. The window with the smallest Δ_m is assumed to be the most similar.

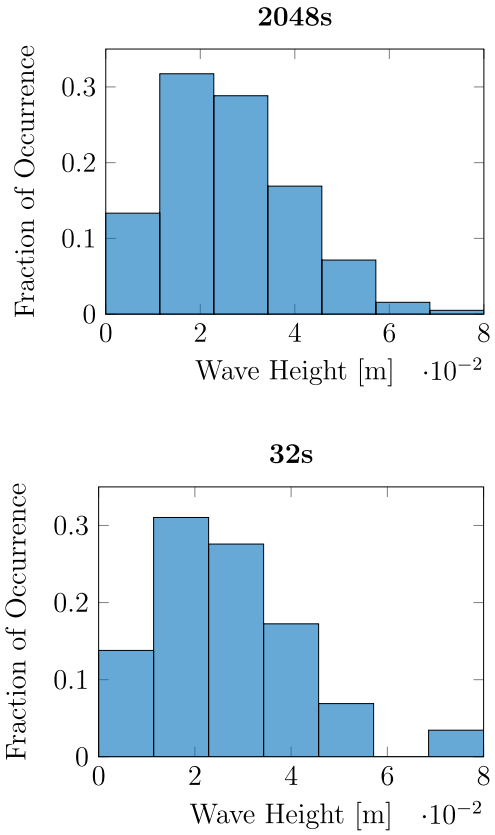

Fig. 5 Histogram of wave heights of a full sea state (top) and similar extract of 32s duration (bottom)

Wave Height Histogram Comparison Method

An alternative metric used is based on the distribution of wave heights. Each sea state has a certain number of waves with respective heights as well as wave lengths which can be displayed graphically in a histogram (Figure 5). It is plotted as the fraction of occurrence (quantity allocated to a bin divided by the total quantity) over the corresponding wave height or period. For the study of power output focus lies on the histogram of wave heights. The bin size is defined for each sea state by dividing the highest wave by seven which also specifies the number of bins. This value was chosen such that histograms of short duration windows with less than thirty waves would still show a reasonable shape. A scalar metric Δ_h can then be computed as follows

$$\Delta_h(w) = \sum_{i=1}^{7} |\beta_i(w) - \beta_{sea,i}| \cdot \varepsilon_i \quad (18)$$

with β_i being the current bin's fraction of occurrence and $\beta_{sea,i}$ the corresponding bin's fraction of the full sea state. The value of the variable ϵ_i is the bin's maximum wave height. They are multiplied to the corresponding absolute difference to add weight to discrepancies of bins with greater wave height, since they are believed to have higher influence on power output.

EXPERIMENTAL SETUP

To investigate the performance of the methods described in the previous sections experimental tank tests were performed. The set up is very sim-

ilar to the one used by Asmuth (2014), so only the most important details are given here. Tests were performed at 40^{th} scale and Froude scaling applied.

The wave tank of the Marine Research Group is 4.58m wide and 20m long. The tank was filled to a water depth of 0.691m from the deepest point. In between the horizontal testing areas, the concrete tank floor gradually slopes up towards the beach. The 20^{th} scale area is located at 6.1m from the paddles and at 0.15m from the deepest point. The 40^{th} scale area starts 12.1m at 0.35m from floor level. In full scale that resembles a water depth of 13.4m for the 40^{th} scale model. See figure 6.

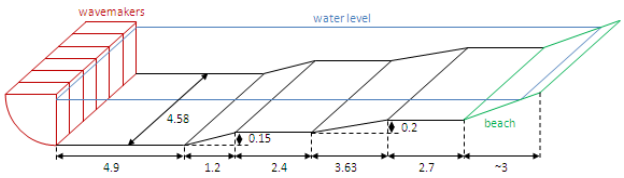

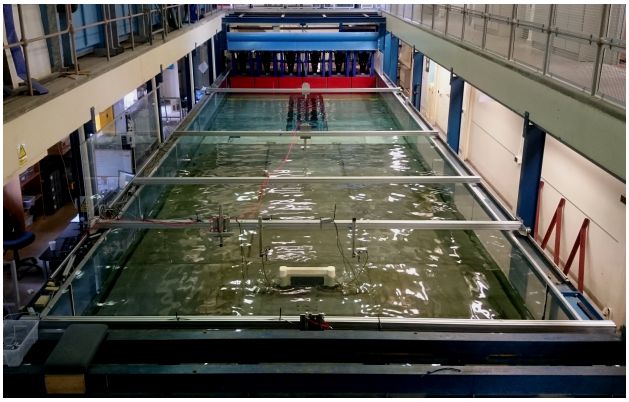

Fig. 6 The QUB wave tank; Schematic drawing of the tank (provided by MRG QUB)(top), photograph from the rear of the tank with model (bottom).

The tank's wave maker module consists of six wave paddles engineered by Edinburgh Design Ltd. Generated waves are mainly absorbed by the beach structure made of geo-textile meshes called Tensamat at the opposite end of the tank. Sensors in the wave paddles detect and absorb reflected waves as well. Detailed information about the tank and beach setup can be found in Henry (2009) and Edinburgh Design Ltd. (2014).

The 40^{th} scale OWSC model designed by Asmuth (2014) was used for the experiments. Its geometries and modifications are shown in Figures 7 and 8. The simple box shaped flap (EE1) can easily be interchanged to a flap with attached end-effectors (EE3) without draining the tank and recalibration of the wave gauges. Therefore different performances of the two designs and the relationship of power output to the given wave trace can be recorded efficiently for each sea state.

The model consists of four foam blocks with aluminium frames for added stability. Furthermore PVC plates compress the foam core. The assembled model is mounted to a bottom tube. Within it lie the torque transducers directly connected to the axis which is held by bearings on the substructure.

Flap rotation, damping torque and surface elevation have been measured at a sampling frequency of 128Hz. The full assembly of equipment is shown in figure 9. The full scale Oyster 800 uses hydraulic pistons to pump pressurized water ashore to the Pelton turbine. Therefore energy is

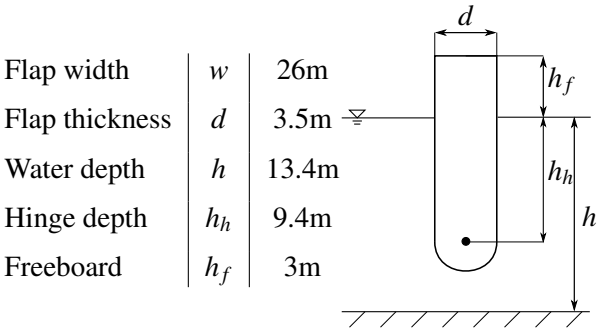

Fig. 7 Definition of geometric parameters in full scale (Asmuth, 2014)

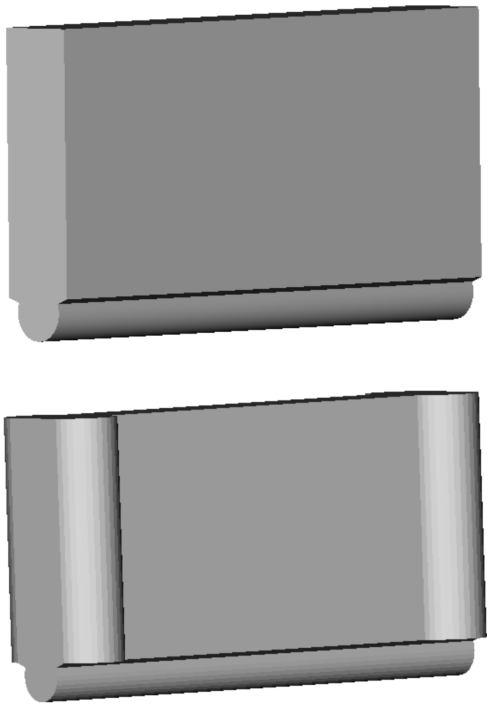

Fig. 8 CAD drawings of investigated flap shapes: flap with square edges (**EE1**, top), flap with additional half-tubes on front and back face (**EE3**,bottom) (Asmuth, 2014)

removed from the wave propelled motion of the device.

To evaluate the performance of a given OWSC different loads are applied to the brakes simulating the power take off system during testing. Torque is measured using custom build torque tubes. Power P is obtained as the product of torque τ times rotational velocity ω.

$$P = \tau \cdot \omega \tag{19}$$

The power curve $P(\tau_{rms})$ is a polynomial fitted trough points of the arithmetic mean of power P over the root mean square (RMS) of instantaneous torque τ_{rms}.

$$\tau_{rms} = \sqrt{\frac{1}{T_r}\int_0^{T_r} [\tau(t)]^2\, dt} \tag{20}$$

Tests were run for different flap shapes and sea states. For each configuration various damping levels were tested to find the optimum level

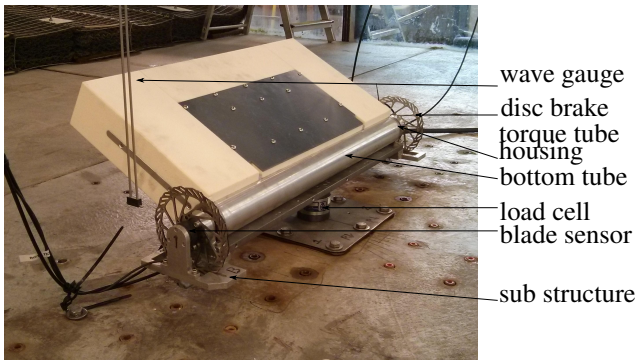

Fig. 9 Setup of model flap, sub structure, damping mechanism and measuring equipment in the wave tank (Asmuth, 2014).

of damping, that is the damping level providing maximum power output. Added end-effectors showed a significant increase of performance compared to the standard flap.

RESULTS

Standard Deviations

The following standard deviation plots include the conventional metrics mean wave height $\bar{H}$, significant wave height $H_{1/3}$ and mean zero up-crossing period T_{zm} in figure 10 as well as maximum power P_{max} and optimum RMS torque τ_{opt} in figure 11. All of which are normalized to the mean of each data point. The standard deviations were deduced from the range of values of the numerous windows analysed. The figures show the convergence of all metrics with increasing window lengths for both modifications of the model.

The individual time domain variables are independent of the tested model, since they are derived from the elevation trace of the sea state. It is noticeable that the standard deviation of the mean zero up-crossing period shows similar values as in the convergence study on fully spectral sea states. The standard deviation of mean and significant wave height of the windows are twice as high. For comparison see fig. 3 and 4.

Optimum RMS torque and maximum power output are influenced by the type of flap used for the experiments. Therefore the standard deviation for both modifications are displayed in figure 11. We see that EE3 causes the values to have a higher standard deviation on the short duration windows, especially for optimum torque.

Evaluation of Method Accuracy

The methods described allow to sort the analysed wave trace windows according to the lowest respective metric of discrepancy under the assumption that the best fit will show a power output very similar to the one deduced from the full 2048s sea state. The methods have been applied to various window lengths, providing a succession of assessed excerpts for each. The "best" window's power output is plotted in the following graphs as circles connected by a solid line over the corresponding window length. The box shaped model is shown in blue and the end-effector model in red. The dashed lines represent the average power output of the entire sea state $P_{max,sea}$, as a reference (Fig. 12, 13).

It is somewhat challenging to asses the quality and the accuracy of each method in a statistical approach. If we look at the ten closest windows $n = 10$ (a small fraction of 0.5-1 % from the quantity of the analysed excerpts) under the assumption that the methods do find excerpts that will produce a more similar power output than a random window, then they should all be close. Therefore it was assumed that the closer the

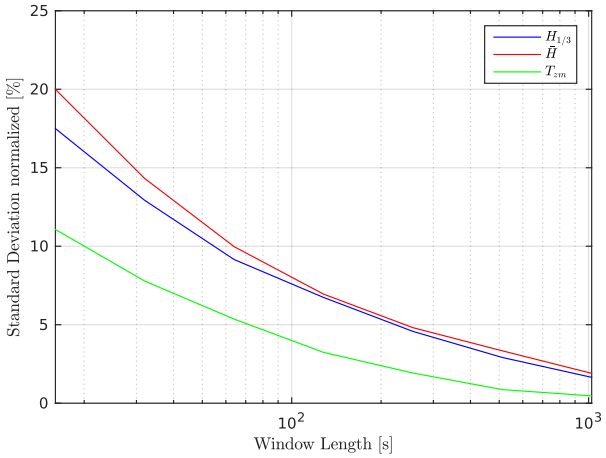

Fig. 10 Standard deviations for individual window lengths of single time domain metrics

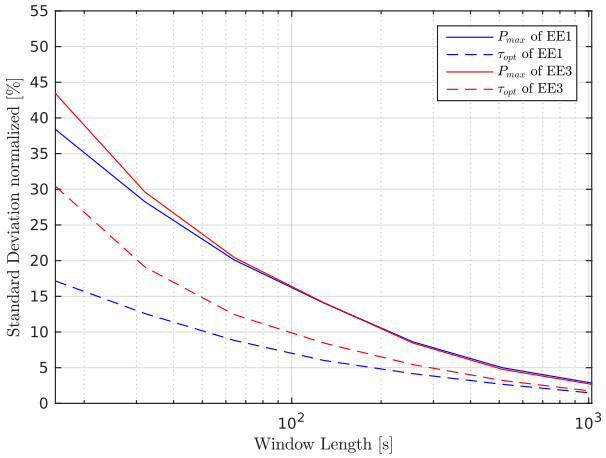

Fig. 11 Standard deviations of torque and power output for varying windowlenghts

best window is to $P_{max,sea}$ and the smaller the standard deviation of the 10 closest windows is, the better the method. A modified standard deviation σ_m was developed to express the average distance of the best window's $P_{max,i}$ to the value of the full sea $P_{max,sea}$.

$$\sigma_m = \sqrt{\frac{\sum_{i=1}^{n}(P_{max,i} - P_{max,sea})^2}{n-1}} \tag{21}$$

σ_m is used given as error-bars for each point and subsequently normalized to $P_{max,sea}$ as displayed with the dash-dotted line.

We observe for both methods that the agreement of the points with the dashed line gets better with growing window length. Also the standard deviation σ_m converges towards zero. Keeping in mind that the standard deviation of P_{max} of all windows behaves likewise this might not be surprising, however if we compare the graphs to figure 11 we see that the methods' standard deviation values of power converge faster. This suggests that they are not scattering much around the desired maximum power output value. The standard deviation of the metric comparison

method does not decline as consistently. A peak is observable at 128s window lengths.

Furthermore it strikes that the curves correlate. Whenever the best window of a certain length overestimates the power output for EE1 it is also overestimated for EE3 by that window in a similar magnitude. The offsets θ are shown in tables 2 and 3 in percent to make this relationship visible.

$$\theta = 1 - \frac{P_{max,i}}{P_{max,sea}} \tag{22}$$

The Pearson correlation coefficient between the offsets of EE1 and EE3 to their respective $P_{max,sea}$ was computed. It was done for the first to the tenth best window of each method to show the continuity of this observation (fig. 14). Values close to 1 describe a strong correlation. The graph shows that for both methods the correlation factor is never lower than 0.94. The offsets of the histogram comparison method have a better correlation in general.

To evaluate which of the two presented methods yields more accurate results the arithmetic mean of the absolute offset

$$\Theta = \frac{\sum_{i=1}^{n} |1 - \frac{P_{max,i}}{P_{max,sea}}|}{n} \tag{23}$$

of the 10 best windows for each window length has been evaluated for each method respectively. As a reference the same has been done for all windows. The result is shown in figure 15. It can be observed that the mean absolute offset of both methods are similar and significantly lower than the mean absolute offset of a randomly chosen window. The curve of the wave height histogram comparison method declines more steadily than the one of the metric comparison method. 16s windows in general have a Θ of approx. 30%, the ten best by each method have a Θ of approx. 10%. Windows that are 128s long have a Θ of approx. 12% while the ten best windows of the histogram comparison method have a Θ of approx. 4%. The arithmetic mean of the absolute offset converges towards zero more rapidly for the excerpts identified by the methods developed in this work than it does for the excerpts as a whole. The methods identify excerpts that are on average 30% closer to the reference power output than a randomly chosen excerpt. Short duration wave traces of 32s achieve Θ values of less than 10%.

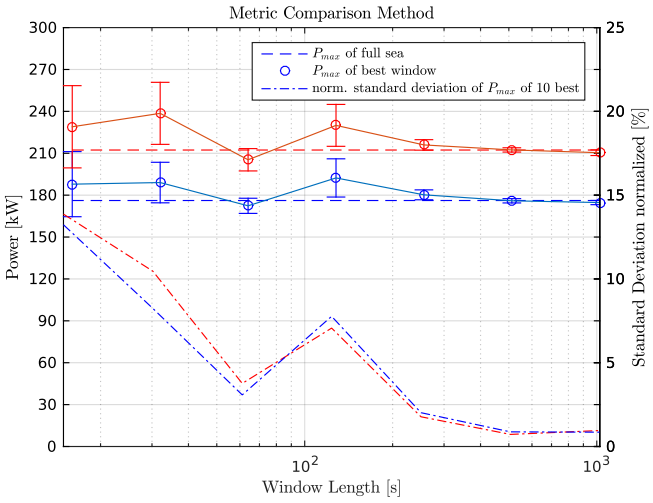

Fig. 12 Power output of best window found with *metric* comparison method over window length. Standard deviation of 10 best windows shown as error bars, blue EE1 and red EE3

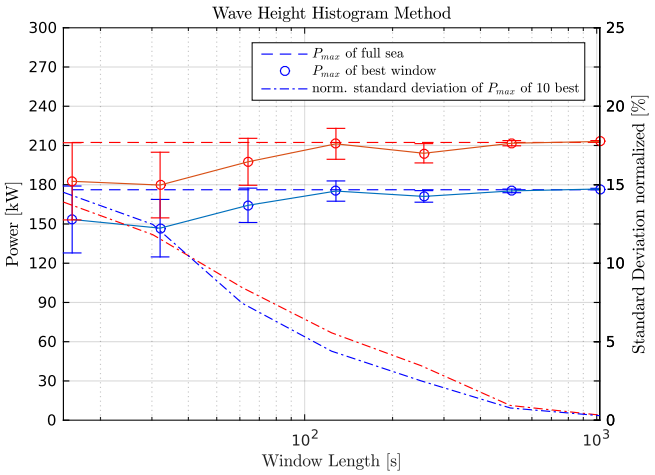

Fig. 13 Power output for the best window found with *histogram method* over window length. Standard deviation of 10 best windows shown as error-bars, blue EE1 and red EE3

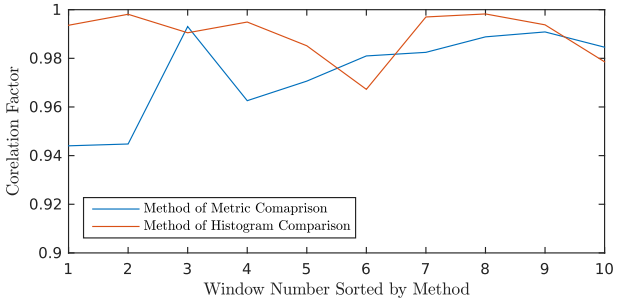

Fig. 14 Correlation between EE1 and EE2 curve of optimum power from fig. 12 and fig. 13 for 10 best windows

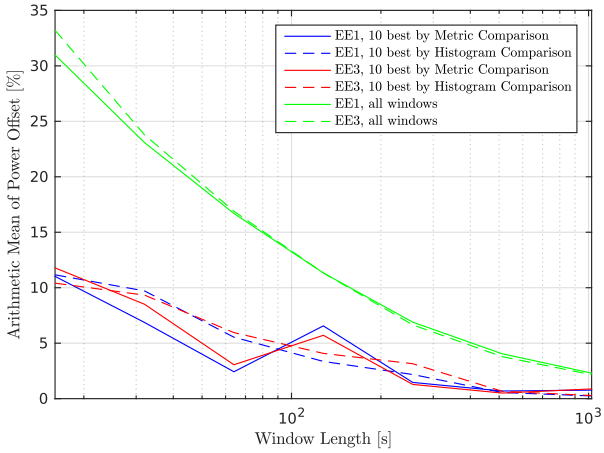

Fig. 15 Arithmetic mean of absolute power offset Θ of 10 best windows of each method and of all windows as a reference line.

Table 2 Offset from maximum power of full sea for best windows of *metric comparison method*

		Window Length [s]						
		16	32	64	128	256	512	1024
Offset θ[%]	EE1	6.64	7.30	-2.16	9.18	2.31	-0.11	-0.83
	EE3	7.84	12.37	-3.28	8.32	1.72	0.038	-0.90

Table 3 Offset from maximum power of full sea for best windows of *histogram comparison method*

		Window Length [s]						
		16	32	64	128	256s	512	1024
Offset θ[%]	EE1	-12.90	-16.67	-6.76	0.57	-2.89	-0.50	0.33
	EE3	-13.99	-15.34	-6.96	-0.49	-3.89	-0.26	0.34

CONCLUSIONS

This paper presents an investigation into the assessment of power output of different OWSC designs using short duration wave traces. Short duration windows can be used to evaluate relative improvement of performance for design changes on model shapes with significant differences. The methods developed in this work are capable of providing wave traces for CFD that achieve a power output value with an accuracy of approx. 10% for windows of 32s or longer and 5% for windows of 128s or longer. The methods are able to evaluate short duration excerpts of the full sea state and filter out windows that would lead to a closer estimation of the maximum power output than a random window would. The wave height histogram comparison method generally show a more consistent decline of its mean absolute offset of the ten closest windows to the histogram of the full sea state.

As the research on metrics describing single waves or wave groups is developing continuously, more metrics become available for testing. A metrics suitability is also likely to depend on the mode of operation of the WEC (or off shore structure). Additional experiments are required to investigate the dependency of the bandwidth of the spectrum. A greater variety of model shapes may be included with shapes of greater and finer difference to make an assumption on the information value delivered by the power production assessment with the developed methods.

Excerpts exist within a full sea state that match the maximum power output within a few percent. Whether they do so by pure chance or by distinctive properties should be reviewed in more detail.

A CFD evaluation of a WEC designs using short duration wave traces of manageable length may now be conducted. The required simulation time can be adjusted dynamically until the difference between two design can be established within the levels of confidence.

ACKNOWLEDGEMENTS

Lucas Danisch's work was supported by the Mobility fund of TU Hamburg Harburg. Their support is much appreciated.

References

Aquamarine Power Ltd (2015). www.aquamarinepower.com.

Asmuth, H. (2014). The influence of end effector shape on the dynamics of the oscillating wave surge converter oyster. Master's thesis, University of Technology Hamburg.

Cameron, L., Doherty, R., Henry, A., Doherty, K., van't Hoff, J., Kaye, D., Naylor, D., Bourdier, S., and Whittaker, T. (2010). Design of the next generation of the oyster wave energy converter. *3rd International Conference on Ocean Energy, 6 October, Bilbao*.

Edinburgh Design Ltd. (2014). www.edesign.co.uk.

Goda, Y. (2010). *Random Seas and Design of Maritime Structures*. World Scientific.

Hasselmann et al. (1973). Measurements of wind-wave growth and swell decay during the joint north sea wave project (jonswap).

Henry, A. (2009). *The hydrodynamics of small seabed mounted bottom hinged wave energy converters in shallow water*. PhD thesis, Queen's University Belfast.

Ochi, M. K. (1998). *Ocean Waves*. Cambridge University Press.

Schmitt, P. and Elsaesser, B. (2015). On the use of openfoam to model oscillating wave surge converters. *Ocean Engineering*. In preparation.

Schmitt, P., Whittacker, T., Clabby, D., and Doherty, K. (2012). The oppurtunities and limitations of using cfd in the developement of waver energy converters. *Marine & Offshore Renewable Energy Conference, London*.